INSTITUTE OF PHYSICS PUBLISHING MODELLING AND SIMULATION IN MATERIALS SCIENCE AND ENGINEERING

Modelling Simul. Mater. Sci. Eng. **15** (2007) S1–S12 doi:10.1088/0965-0393/15/1/S01

Strain gradient effects in surface roughening

Ulrik Borg[1] **and Norman A Fleck**[2]

[1]Department of Mechanical Engineering, Technical University of Denmark, 2800 Kgs. Lyngby, Denmark
[2]Engineering Department, Cambridge University, Trumpington Street, Cambridge CB2 1PZ, UK

E-mail: ub@mek.dtu.dk

Received 4 May 2006, in final form 28 August 2006
Published 6 December 2006
Online at stacks.iop.org/MSMSE/15/S1

Abstract

A thin aluminium sheet comprising of large polycrystals is pulled in uniaxial tension and the resulting surface profile is measured in a scanning electron microscope. The surface profile near the grain boundaries reveals a local deformation pattern of width of a few micrometres and is strong evidence for strain gradient effects. Numerical analyses of a bicrystal undergoing in-plane tensile deformation are also studied using a strain gradient crystal plasticity theory and also by using a strain gradient plasticity theory for an isotropic solid. Both theories include an internal material length scale. An interfacial potential that penalizes the dislocations in crossing the grain boundary is included in the analysis. The results indicate that the surface profile is strongly dependent upon the choice of this potential and on the material length scale.

1. Introduction

Surface roughening of polycrystalline metals during plastic deformation is a common phenomenon in metal forming processes and is commonly referred to as the 'orange peel' effect. In addition to creating cosmetically undesirable surfaces, the inhomogeneities can provide initiation sites for fatigue crack initiation and strain localization. The effect derives from the crystallographic lattice mismatch from grain to grain and the resulting anisotropy in different grains. Incompatibilities of deformation from the interaction between adjacent grains result in the roughening of the free surface.

The surface roughening of polycrystalline Al–Mg alloys during tensile deformation has been experimentally studied by, for example, Stoudt and Ricker (2002). It was observed that the degree of surface roughening increases linearly with both grain size and level of imposed strain. However, an extrapolation of the data to vanishing grain size gives a finite surface roughening and this suggests that an independent material length scale influences the surface roughening in addition to the grain size. Wilson and Lee (2001) made observations of aluminium alloy surfaces deformed in tension, sheet forming and rolling. They observed the

formation of valleys near grain boundaries and concluded that this was a result of the mismatch in the orientation of slip systems of adjacent grains. The width of the valleys were on the order of 3 μm with grain sizes of 15 μm for a surface rolled to 30% reduction.

Numerical simulations based on crystal plasticity finite element models have been widely used to study surface roughening in polycrystals (see e.g. Zhao *et al* (2004) using a three-dimensional conventional crystal plasticity model). The results indicate that the dispersion of crystallographic texture from grain to grain plays an important role in surface roughening. Most of such analyses have been based on several crystals, and have not focused on the local deformation field near surface grain boundaries.

The grain boundary obstructs the motion of dislocations and results in local gradients in plastic strain. In strain gradient plasticity formulations it is possible to introduce an energy term acting at an interface in order to constrain the plastic flow across the interface. Aifantis and Willis (2005) employ the framework of Fleck and Willis (2004) but introduce an interfacial energy potential to penalize the build-up of plastic strain at interfaces. This induces a jump in the higher order tractions and plastic strain gradients but a continuity of plastic strain across the interface. A similar approach has been used by Gudmundson (2004) that allows for jumps in higher order tractions and plastic strains and by Evers *et al* (2004) who uses an enhanced crystal plasticity framework based on various types of dislocation densities allowing for jumps in dislocation densities at grain boundaries. Furthermore, Gurtin and Needleman (2005) have discussed the conditions for a continuous distribution of Burgers vector across a boundary.

The numerical analyses in the present study are based on a rate-dependent strain gradient crystal plasticity formulation as presented by Borg (2006). It sits within the framework of the phenomenological strain gradient theory by Fleck and Hutchinson (2001). Here, the formulation is enhanced by introducing a potential that penalizes crystallographic slip at internal grain boundaries. The potential is a function of the slips on either side of the grain boundary. This formulation admits jumps in the higher order tractions and slips but has continuity of displacement across grain boundaries.

For comparison purposes some of the simulations are obtained using the viscoplastic strain gradient plasticity theory for an isotropic solid based upon Fleck and Hutchinson (2001), as presented in Borg *et al* (2006). No interfacial potential is used in that case, although it would be possible to formulate one.

2. Experiments

Uniaxial tension tests have been conducted on commercially pure aluminium in order to observe the surface profile near grain boundaries during plastic deformation. The specimen was prepared by prescribing 4% tensile pre-strain to an annealed, cold rolled sheet of length 120 mm, width 20 mm and thickness 1.2 mm. The sheet was then given a recrystallization anneal at 540 °C for 15 min, and the resulting grain structure comprised through-thickness pancake-shaped grains of average diameter 5 mm. The surface of the specimens was mechanically polished prior to deformation. A scanning electron microscope (SEM) was used to investigate the surface profile. Figure 1 displays two SEM images of the surface after 10 per cent engineering strain. On the left image a grain boundary has been marked to emphasize the jump in surface profile across the grain boundary. The image on the right shows a grain boundary and slip lines on either side of it. The grains on each side clearly have different crystallographic orientations, and the density of slip lines is increased on one side of the grain boundary.

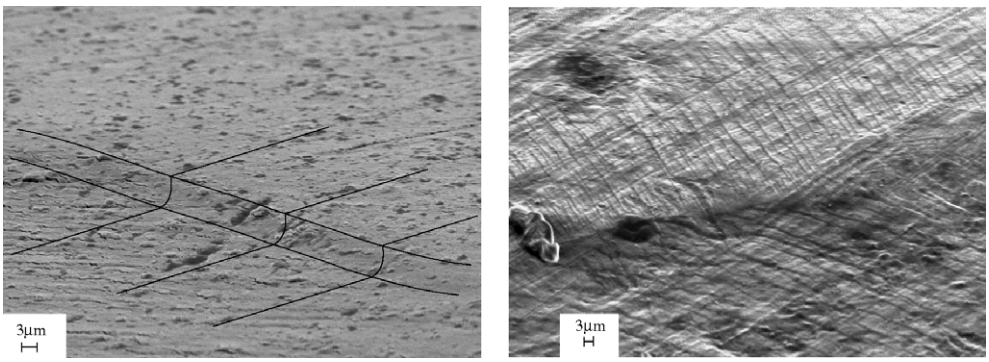

Figure 1. SEM images of the surface after 10% strain.

3. Material model

Results will be based mainly on the strain gradient crystal plasticity theory for finite deformations presented by Borg (2006). The formulation fits within the framework of the strain gradient theory by Fleck and Hutchinson (2001) with the basic formulation equivalent to Gurtin (2002) and reduces to the conventional crystal plasticity theory by, for example, Peirce *et al* (1983) in the absence of strain gradients. A new interfacial potential is introduced to account for the grain boundary resistance to dislocations. For comparison purposes we also present results using a strain gradient plasticity theory for an isotropic solid. The formulation used is a viscoplastic version of the theory by Fleck and Hutchinson (2001) as presented by Borg *et al* (2006). For the isotropic phenomenological solid no interfacial potential is introduced. However, various higher order boundary conditions are assumed to explore their effect upon the surface profile. In the following summaries of the two formulations, the small strain theory is assumed for the sake of simplicity and clarity, although a full finite deformation formulation has been used in all calculations.

3.1. Strain gradient crystal plasticity theory

Plastic deformation by crystallographic slip represents dislocation motion along specific slip systems. A slip system (α) is described by its lattice vectors $s_i^{(\alpha)}$ and $m_i^{(\alpha)}$, where $s_i^{(\alpha)}$ is the slip direction and $m_i^{(\alpha)}$ is the direction normal to the slip plane. Upon introducing $\mu_{ij}^{(\alpha)} = \frac{1}{2}(s_i^{(\alpha)} m_j^{(\alpha)} + s_j^{(\alpha)} m_i^{(\alpha)})$ as the classical Schmid orientation tensor, the overall macroscopic plastic strain rate components can be expressed by the slip $\gamma^{(\alpha)}$ along slip system (α) as

$$\dot{\epsilon}_{ij}^{p} = \sum_{\alpha} \dot{\gamma}^{(\alpha)} \mu_{ij}^{(\alpha)}. \tag{1}$$

An effective slip measure $\gamma_{\mathrm{e}}^{(\alpha)}$ depending on the slip and the slip gradients is introduced as

$$\dot{\gamma}_{\mathrm{e}}^{(\alpha)^2} = \dot{\gamma}^{(\alpha)^2} + (l_S \dot{\gamma}_{,i}^{(\alpha)} s_i^{(\alpha)})^2 + (l_M \dot{\gamma}_{,i}^{(\alpha)} m_i^{(\alpha)})^2 + (l_T \dot{\gamma}_{,i}^{(\alpha)} t_i^{(\alpha)})^2, \tag{2}$$

where $t_i^{(\alpha)}$ is the transverse direction and l_S, l_M and l_T are material length scales introduced for dimensional consistency. Here, $(\,)_{,i} = \partial/\partial x_i$ is the spatial derivative. In this work, only plane problems with in-plane slip systems are considered, and therefore the contribution from the slip gradient in the transverse direction is neglected in the following.

To account for the grain boundary resistance to dislocations crossing them, two surface energy potentials $\phi_{\mathrm{I}}^{(\alpha)}(\gamma_{\mathrm{I}}^{(\alpha)})$ and $\phi_{\mathrm{II}}^{(\alpha)}(\gamma_{\mathrm{II}}^{(\alpha)})$ acting at side 1 and side 2 of the grain boundary Γ,

respectively, are introduced. Then, the principle of virtual power takes the form (where $\phi_{\rm I}^{(\alpha)\prime}$ denotes $\partial\phi_{\rm I}^{(\alpha)}/\partial\gamma_{\rm I}^{(\alpha)}$, etc)

$$\int_V \left(\sigma_{ij}\delta\dot{\epsilon}_{ij} + \sum_\alpha \left(Q^{(\alpha)} - \tau^{(\alpha)}\right)\delta\dot{\gamma}^{(\alpha)} + \sum_\alpha \left(\xi_S^{(\alpha)} s_i^{(\alpha)} + \xi_M^{(\alpha)} m_i^{(\alpha)}\right)\delta\dot{\gamma}_{,i}^{(\alpha)} \right) \mathrm{d}V + \int_\Gamma \sum_\alpha \left(\phi_{\rm I}^{(\alpha)\prime}\delta\dot{\gamma}_{\rm I}^{(\alpha)} + \phi_{\rm II}^{(\alpha)\prime}\delta\dot{\gamma}_{\rm II}^{(\alpha)}\right) \mathrm{d}\Gamma = \int_S \left(T_i\delta\dot{u}_i + \sum_\alpha r^{(\alpha)}\delta\dot{\gamma}^{(\alpha)} \right) \mathrm{d}S. \quad (3)$$

Here, $Q^{(\alpha)}$ is a stress field work conjugate to the slip rate, and the higher order stresses $\xi_S^{(\alpha)}$ and $\xi_M^{(\alpha)}$ are work conjugate to the slip rate gradients along the slip direction and the direction normal to the slip plane, respectively. T_i is the stress traction and $r^{(\alpha)}$ denotes the higher order traction working on the part of the boundary S where the displacement rates $\dot{u}_i$ and slip rates $\dot{\gamma}^{(\alpha)}$ are not prescribed. The Cauchy stress is denoted σ_{ij} and $\tau^{(\alpha)} = \sigma_{ij}\mu_{ij}^{(\alpha)}$ is the Schmid stress.

It is assumed that the total displacement fields are continuous across the grain boundary but that the presence of a grain boundary energy term causes jumps in the slips. Full constraint along Γ with $\gamma^{(\alpha)} = 0$ is obtained by letting $\phi_{\rm I}^{(\alpha)\prime}$ and $\phi_{\rm II}^{(\alpha)\prime}$ tend to infinity, whereas vanishing surface energy along Γ mimics that dislocations are free to cross the grain boundary.

The strong form of the field equations is found by requiring the above relation to hold for all admissible variations in $\dot{u}_i$ and $\dot{\gamma}^{(\alpha)}$. The classical force balance law and boundary conditions read as

$$\sigma_{ij,j} = 0 \qquad T_i = \sigma_{ij}n_j, \quad (4)$$

where n_i is the surface unit normal in the deformed configuration. In addition, we have the consistency condition and higher order boundary conditions

$$Q^{(\alpha)} - \tau^{(\alpha)} - \xi_{S,i}^{(\alpha)} s_i^{(\alpha)} - \xi_{M,i}^{(\alpha)} m_i^{(\alpha)} = 0 \quad (5)$$

$$r^{(\alpha)} = \left(\xi_S^{(\alpha)} s_i^{(\alpha)} + \xi_M^{(\alpha)} m_i^{(\alpha)}\right) n_i. \quad (6)$$

The interface conditions are given by

$$\left[\sigma_{ij}N_j\right] = 0, \quad (7)$$

$$\left(\xi_S^{(\alpha){\rm I}} s_i^{(\alpha){\rm I}} + \xi_M^{(\alpha){\rm I}} m_i^{(\alpha){\rm I}}\right) N_i = \phi_{\rm I}^{(\alpha)\prime}(\gamma_{\rm I}^{(\alpha)}), \quad (8)$$

$$\left(\xi_S^{(\alpha){\rm II}} s_i^{(\alpha){\rm II}} + \xi_M^{(\alpha){\rm II}} m_i^{(\alpha){\rm II}}\right) (-N_i) = \phi_{\rm II}^{(\alpha)\prime}(\gamma_{\rm II}^{(\alpha)}), \quad (9)$$

where the unit normal vector N_i on Γ is directed from grain 1 to grain 2 and $[f]$ denotes the jump $f_1 - f_2$ across Γ. Simple expressions are adopted for the grain boundary energy potentials of the form

$$\phi_{\rm I}^{(\alpha)} = \frac{1}{2}\kappa(\gamma_{\rm I}^{(\alpha)})^2, \qquad \phi_{\rm I}^{(\alpha)\prime} = \kappa\gamma_{\rm I}^{(\alpha)}, \quad (10)$$

$$\phi_{\rm II}^{(\alpha)} = \frac{1}{2}\kappa(\gamma_{\rm II}^{(\alpha)})^2, \qquad \phi_{\rm II}^{(\alpha)\prime} = \kappa\gamma_{\rm II}^{(\alpha)}, \quad (11)$$

with κ being a material parameter describing the strength of the grain boundary.

By use of an effective stress, denoted $\tau_{\rm e}^{(\alpha)}$, that is work-conjugate to the effective slip rate measure, $\dot{\gamma}_{\rm e}^{(\alpha)}$, a power-law creep model is formulated as

$$\dot{\gamma}_{\rm e}^{(\alpha)} = \dot{\gamma}_0 \left(\frac{\tau_{\rm e}^{(\alpha)}}{g^{(\alpha)}}\right)^{1/m}, \quad (12)$$

where $\dot{\gamma}_0$ is a reference slip rate and m is a strain rate hardening index. The slip resistance $g^{(\alpha)}$ is assumed to harden from an initial value τ_0 according to

$$\dot{g}^{(\alpha)} = \sum_{\beta} h_{\alpha\beta}\dot{\gamma}_{\mathrm{e}}^{(\beta)}, \qquad h_{\alpha\beta} = h\delta_{\alpha\beta} + ph\left(1 - \delta_{\alpha\beta}\right), \tag{13}$$

where p is the latent hardening index, h is the self-hardening modulus and $\delta_{\alpha\beta}$ denotes the Kronecker delta symbol. Here, we use Taylor hardening ($p = 1$) and linear hardening ($h = h_0 =$ constant).

3.2. Strain gradient viscoplastic theory for an isotropic solid

A much simpler, phenomenological strain gradient formulation exists for an isotropic elastic–plastic solid. Introduce a nonlocal measure of the effective plastic strain rate $\dot{E}^P$ on the basis of the conventional effective plastic strain rate $\dot{\epsilon}^P$ and its gradient through the incremental relation

$$\dot{E}^{P^2} = \dot{\epsilon}^{P^2} + l^2\dot{\epsilon}^P_{,i}\dot{\epsilon}^P_{,i}, \tag{14}$$

where l is a material length parameter. The direction of the plastic strain rate is given by $m_{ij} = \frac{3}{2}S_{ij}/\sigma_{\mathrm{e}}$, where $S_{ij} = \sigma_{ij} - \frac{1}{3}\delta_{ij}\sigma_{kk}$ denotes the stress deviator and $\sigma_{\mathrm{e}} = \sqrt{\frac{3}{2}S_{ij}S_{ij}}$ is the von Mises effective stress and σ_{ij} is the Cauchy stress tensor. The plastic strain rate components can then be written as a product of its magnitude, $\dot{\epsilon}^P = \sqrt{\frac{2}{3}\dot{\epsilon}^P_{ij}\dot{\epsilon}^P_{ij}}$ and its direction m_{ij} as $\dot{\epsilon}^P_{ij} = m_{ij}\dot{\epsilon}^P$.

Now follow Fleck and Hutchinson (2001) and assume that the plastic strain gradients contribute to the internal work. Then, the principle of virtual power takes the form

$$\int_V \left(\sigma_{ij}\delta\dot{\epsilon}^{EL}_{ij} + Q\delta\dot{\epsilon}^P + \tau_i\delta\dot{\epsilon}^P_{,i}\right)\mathrm{d}V = \int_S \left(T_i\delta\dot{u}_i + r\delta\dot{\epsilon}^P\right)\mathrm{d}S \tag{15}$$

in the deformed configuration. Here, $\epsilon^{\mathrm{EL}}_{ij}$ is the elastic strain, Q is a generalized effective stress which is work-conjugate to the conventional effective plastic strain rate, $\dot{\epsilon}^P$, and τ_i is a higher order stress which is work-conjugate to the gradient of the conventional effective plastic strain rate, $\dot{\epsilon}^P_{,i}$. Integration by parts of this work equation leads to the identity $Q = \sigma_{\mathrm{e}} + \tau_{i,i}$. The surface stress traction is given by $T_i = \sigma_{ij}n_j$, and r denotes the higher order surface traction.

The viscous material behaviour is modelled by a power law for the effective plastic strain rate

$$\dot{E}^P = \dot{\epsilon}_0\left(\frac{\sigma_{\mathrm{c}}}{g(E^P)}\right)^{1/m}. \tag{16}$$

Here, m is the strain rate hardening exponent, $\dot{\epsilon}_0$ is a reference strain rate and σ_c is an effective stress which is work-conjugate to the effective plastic strain rate $\dot{E}^P$ such that

$$\sigma_{\mathrm{c}}\delta\dot{E}^P = Q\delta\dot{\epsilon}^P + \tau_i\delta\dot{\epsilon}^P_{,i}. \tag{17}$$

The hardening function g is taken as

$$g(E^P) = \sigma_0 + h_0E^P, \tag{18}$$

where σ_0 is the initial yield strength and h_0 is the hardening modulus.

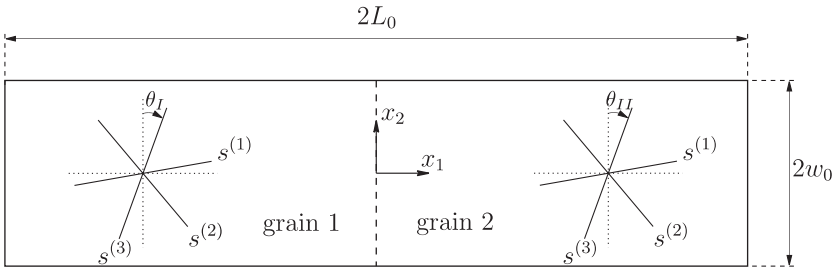

Figure 2. The bicrystal considered in the analyses with three slip systems.

4. Numerical method and modelling details

A bicrystal undergoing in-plane tensile deformation is studied. As shown in figure 2 the bicrystal consists of two grains infinitely long in the x_3-direction separated by a grain boundary at $x_1 = 0$. In the crystal plasticity calculations we use a planar model with three slip systems at a relative orientation of 60° from one to the next. Their absolute orientation is given by the angles $\theta_{\rm I}$ and $\theta_{\rm II}$ between slip system three and the x_2-direction. The slip system orientation $\theta = 0$ is close to an FCC material under plane strain tension in the $\langle 110 \rangle$ direction which can be simulated with three slip systems oriented at $\pm 35.3°$ and 90° from the tensile axis (see e.g. Rice (1987)). To mimic different crystal orientations, results are presented with varying values of θ.

The applied boundary conditions are given by

$$\begin{array}{lll} \dot{u}_1 = 0, \quad \dot{T}_2 = 0 & \text{at } \mathrm{x_1} = -\mathrm{L_0}, \\ \dot{u}_1 = \dot{U}, \quad \dot{T}_2 = 0 & \text{at } \mathrm{x_1} = \mathrm{L_0}, \\ \dot{T}_1 = 0, \quad \dot{T}_2 = 0 & \text{at } \mathrm{x_2} = -\mathrm{w_0}, \\ \dot{T}_1 = 0, \quad \dot{T}_2 = 0 & \text{at } \mathrm{x_2} = \mathrm{w_0}, \end{array} \tag{19}$$

where $\dot{U}$ is the applied end displacement rate. Furthermore, the higher order tractions $r^{(\alpha)}$ vanish on the external boundary.

The numerical solutions are obtained using the finite element method. The slip rate increments and plastic strain rate increments for the crystal formulation and isotropic formulation, respectively, are primary unknowns on an equal footing with the displacement increments. These primary unknowns are interpolated within each element between nodal increments as

$$\Delta u_i = \sum_{N=1}^{2k} N_i^N \Delta D^N, \qquad \Delta \dot{\gamma}^{(\alpha)} = \sum_{N=1}^{l} M^N \Delta \dot{\gamma}_N^{(\alpha)} \tag{20}$$

for the crystal formulation, and for the isotropic formulation as

$$\Delta u_i = \sum_{N=1}^{2k} N_i^N \Delta D^N, \qquad \Delta \dot{\epsilon}^P = \sum_{N=1}^{l} M^N \Delta \dot{\epsilon}_N^P, \tag{21}$$

where N_i^N and M^N are shape functions and k and l are the number of nodes used for the interpolations. The elements used for the displacements are 8-node quadrilaterals with quadratic shape functions, and the elements used for interpolation of the slip rate increments or plastic strain rate increments are 4-node quadrilaterals with linear shape functions, i.e. $k = 8$ and $l = 4$.

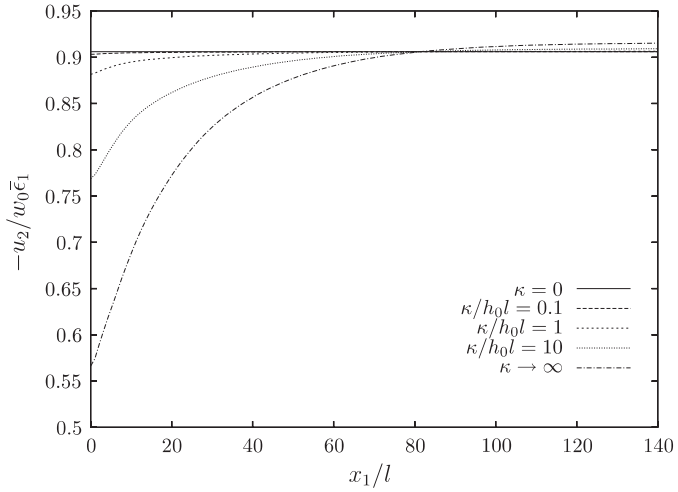

Figure 3. The surface profile near the grain boundary for a bicrystal with $\theta_{\mathrm{I}} = \theta_{\mathrm{II}} = 0$ and the same material parameters for $l/w_0 = 0.01$ at $\bar{\epsilon}_1 = 5\%$.

To allow for discontinuity of slips at the grain boundary, double nodes for the slips must be present at the grain boundary. In this way the slip on each slip system is uncoupled on the two sides of the boundary. In contrast, the displacements are coupled to ensure continuity of the total strain field.

5. Results

The material parameters used for the crystal plasticity calculations are $\tau_0/E = 0.001$, $h_0/\tau_0 = 10$ and $\dot{\gamma}_0 = 0.001\,\mathrm{s}^{-1}$. For the analyses using the isotropic plasticity theory the material parameters are taken as $\sigma_0/E = 0.002$, $h_0/\sigma_0 = 20$ and $\dot{\epsilon}_0 = 0.001\,\mathrm{s}^{-1}$. Using these material data, the stress–strain responses in plane strain tension for (i) an isotropic material and for (ii) a single crystal with slip systems oriented at $\pm 30^\circ$ and 90° from the tensile axis are identical. In both cases the Poisson's ratio $\nu = 0.3$, and the strain rate hardening index is taken as $m = 0.02$ in order to mimic rate-independent plasticity. The dimensions of the bicrystal are chosen such that the ratio w_0/L_0 is small enough to let us neglect specimen end effects. The applied end displacement rate is given by $\dot{U}/2L_0 = \dot{\gamma}_0$ or $\dot{U}/2L_0 = \dot{\epsilon}_0$ for crystal plasticity and isotropic plasticity, respectively.

It can be argued that a slip gradient in the slip direction can be related to edge dislocations, that a slip gradient in the transverse direction (which is absent in this plane problem) can be related to screw dislocations and that a slip gradient in the direction normal to the slip plane, $\gamma^{(\alpha)}_{,i} m^{(\alpha)}_i$, does not induce any geometrical necessary dislocations and thus it should not contribute to the hardening. Therefore we have used $l_M = 0$ in all the calculations, and the other material length scale l_{S} is denoted as l. Unless otherwise stated, the following results have been obtained using the crystal plasticity formulation.

First, a bicrystal is studied such that the two grains have the same orientation of slip systems ($\theta_{\mathrm{I}} = \theta_{\mathrm{II}} = 0$) and the same material parameters. The surface profile at an overall strain $\bar{\epsilon}_1 = U/2L_0 = 5\%$ is shown in figure 3 for $l/w_0 = 0.01$ and in figure 4 for $l/w_0 = 0.1$. Due to symmetry the profiles are only shown for $x_1 \geqslant 0$. In each figure results are displayed for five values of the parameter κ characterizing the grain boundary. For $\kappa = 0$ there is a homogeneous deformation state throughout the specimen, and the surface profile is level.

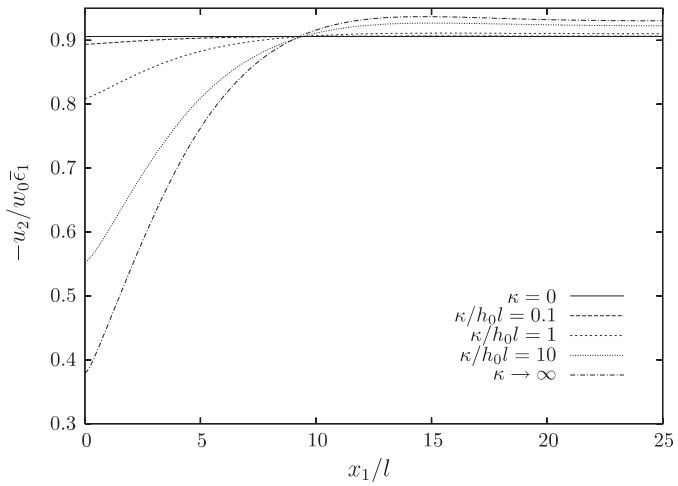

Figure 4. The surface profile near the grain boundary for a bicrystal with $\theta_{\rm I} = \theta_{\rm II} = 0$ and the same material parameters for $l/w_0 = 0.1$ at $\bar{\epsilon}_1 = 5$.

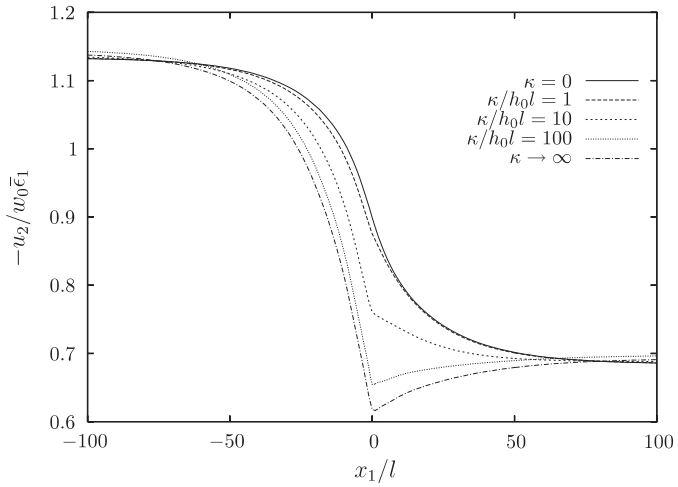

Figure 5. The surface profile near the grain boundary for a bicrystal with $\theta_{\rm I} = \theta_{\rm II} = 0$ and initial slip resistances $\tau_0^{\rm II}/\tau_0^{\rm I} = 2$ for $l/w_0 = 0.01$ at $\bar{\epsilon}_1 = 5\%$.

The curve marked as $\kappa \to \infty$ is obtained using $\gamma^{(\alpha)} = 0$, simulating a grain boundary that is impenetrable to dislocations. Note that an increased value of κ constrains the slips, and thereby the plastic strains, leading to a decrease in the lateral displacement of the specimen at the grain boundary. Figures 3 and 4 illustrate this: there is an increase in the profile at the grain boundary as the value of κ increases.

Figures 5 and 6 show surface profiles for a bicrystal where the two grains have the same crystallographic orientation but the initial slip resistance in grain 1 is half that of grain 2 ($\tau_0^{\rm II}/\tau_0^{\rm I} = 2$), for $l/w_0 = 0.01$ and $l/w_0 = 0.1$. Results are presented for five values of κ at an axial strain of $\bar{\epsilon}_1 = 5\%$. The height of the surface for $\kappa = 0$ (the solid line) decreases monotonically from the strong grain to the weak grain for both values of l/w_0. For $\kappa \to \infty$ the profiles contact a re-entrant corner at the grain boundary, due to the restriction on slips.

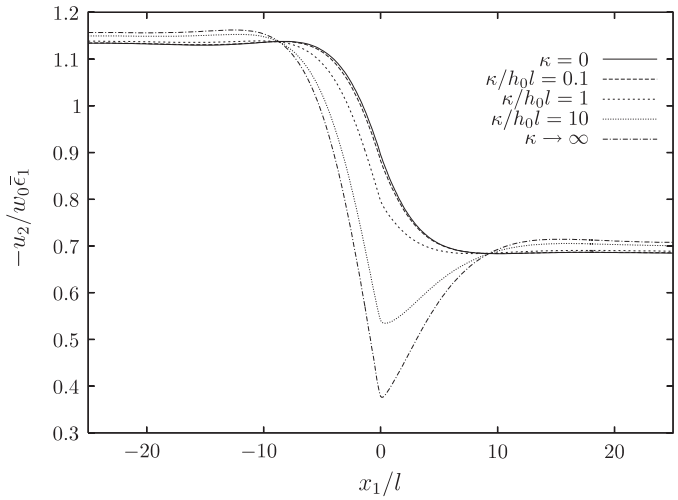

Figure 6. The surface profile near the grain boundary for a bicrystal with $\theta_{\mathrm{I}} = \theta_{\mathrm{II}} = 0$ and initial slip resistances $\tau_0^{\mathrm{II}}/\tau_0^{\mathrm{I}} = 2$ for $l/w_0 = 0.1$ at $\bar{\epsilon}_1 = 5\%$.

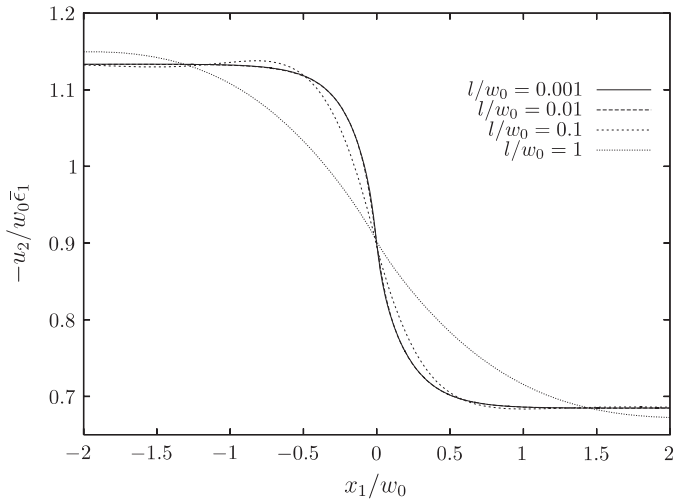

Figure 7. The surface profile near the grain boundary for a bicrystal with $\theta_{\mathrm{I}} = \theta_{\mathrm{II}} = 0$ and initial slip resistances $\tau_0^{\mathrm{II}}/\tau_0^{\mathrm{I}} = 2$ for $\kappa = 0$ at $\bar{\epsilon}_1 = 5\%$.

The sensitivity of the surface profile to the material length scale l/w_0 is shown in figure 7 for $\kappa = 0$ and in figure 8 for $\kappa \to \infty$. These results pertain to the same bicrystal as reported in figures 5 and 6. For the choice $\kappa = 0$ the profile at $l/w_0 = 0.001$ and $l/w_0 = 0.01$ coincide, and only the profile curve for $l/w_0 = 1$ is significantly different from the others. All the profiles with $\kappa = 0$ show a monotonic decrease from the strong grain to the weak grain. In contrast, the value of l/w_0 has a significant effect upon the profiles in figure 8 at $\kappa \to \infty$. For $l/w_0 = 0.001$ the profile is almost constant within the strong grain and decreases within the weak grain, whereas for $l/w_0 = 0.1$ the width of the deformed specimen first increases within the strong grain before it decreases in the weak grain due to the full constraint on slip.

A comparison of surface profiles using strain gradient crystal plasticity and isotropic, phenomenological strain gradient plasticity theory is given in figure 9. The crystal calculations

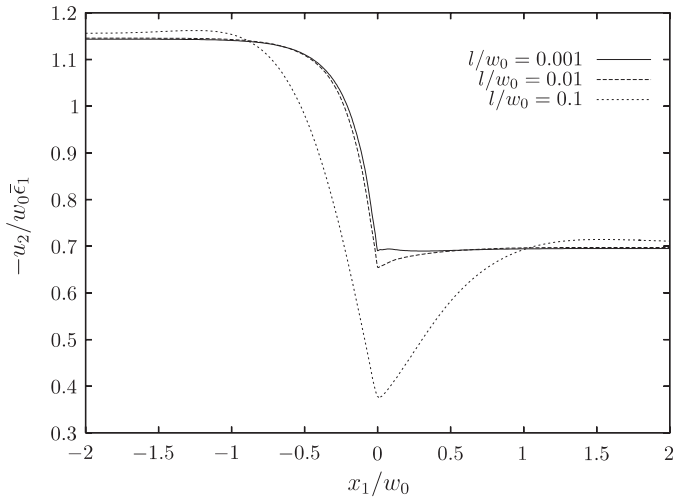

Figure 8. The surface profile near the grain boundary for a bicrystal with $\theta_{\mathrm{I}} = \theta_{\mathrm{II}} = 0$ and initial slip resistances $\tau_0^{\mathrm{II}}/\tau_0^{\mathrm{I}} = 2$ for $\kappa \to \infty$ at $\bar{\epsilon}_1 = 5\%$.

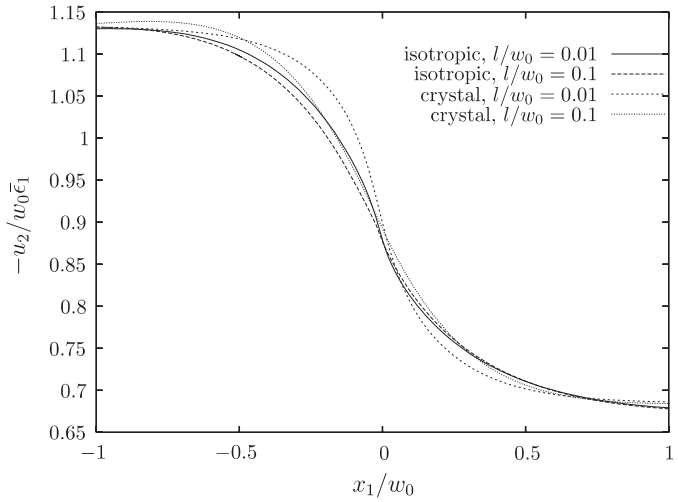

Figure 9. Surface profile near the grain boundary using strain gradient crystal plasticity with $\theta_{\mathrm{I}} = \theta_{\mathrm{II}} = 0$, initial slip resistances $\tau_0^{\mathrm{II}}/\tau_0^{\mathrm{I}} = 2$ and continuity of slips and strain gradient plasticity for an isotropic material having continuity of plastic strains at the interface with $\sigma_0^{\mathrm{II}}/\sigma_0^{\mathrm{I}} = 2$. Both at $\bar{\epsilon}_1 = 5\%$ for two values of l/w_0.

have been carried out for continuity of slips at the grain boundary ($\gamma_{\mathrm{I}}^{(\alpha)} = \gamma_{\mathrm{II}}^{(\alpha)}$) and $\kappa = 0$, i.e. not using double nodes at the grain boundary. This option is only meaningful when the slip systems in the two grains have the same orientation, which is the case for the results presented in figure 9 ($\theta_{\mathrm{I}} = \theta_{\mathrm{II}} = 0$). The initial slip resistances are taken as $\tau_0^{\mathrm{II}}/\tau_0^{\mathrm{I}} = 2$. In the calculations based on the isotropic formulation there is continuity of plastic strains at the grain boundary and the yield strength of the two grains are taken as $\sigma_0^{\mathrm{II}}/\sigma_0^{\mathrm{I}} = 2$. The results show that there is no significant difference in the surface profiles using the two different formulations, although there is a tendency for the crystal profile to have a locally steeper slope than for the isotropic phenomenological solid.

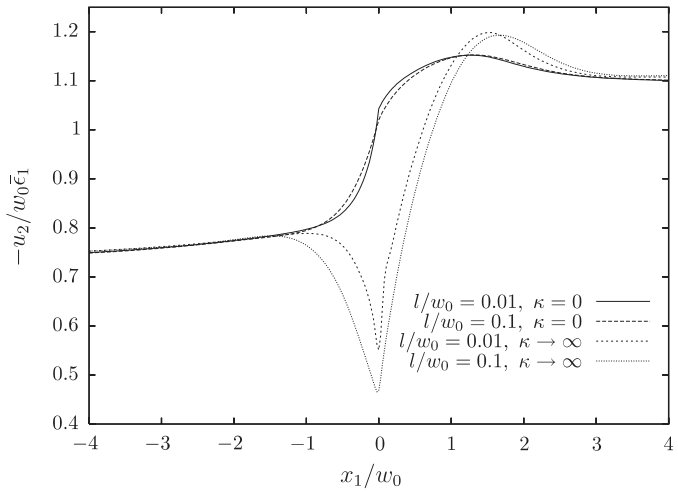

Figure 10. The surface profile near the grain boundary for a bicrystal with $\theta_{\mathrm{I}} = 0^\circ$ and $\theta_{\mathrm{II}} = 15^\circ$ and the same material parameters for $\kappa \to \infty$ and $\kappa = 0$ at $\bar{\epsilon}_1 = 5\%$ for two values of l/w_0.

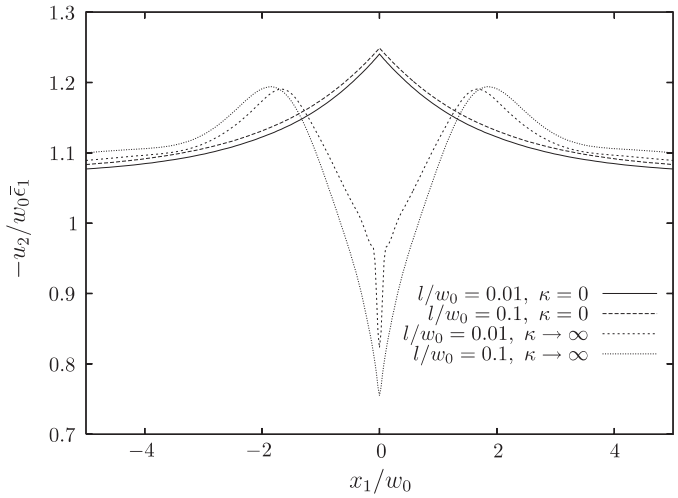

Figure 11. The surface profile near the grain boundary for a bicrystal with $\theta_{\mathrm{I}} = -15^\circ$ and $\theta_{\mathrm{II}} = 15^\circ$ and the same material parameters for $\kappa \to \infty$ and $\kappa = 0$ at $\bar{\epsilon}_1 = 5\%$ for two values of l/w_0.

Next, a bicrystal with a lattice mismatch as specified by $\theta_{\mathrm{I}} = 0^\circ$ and $\theta_{\mathrm{II}} = 15^\circ$ is considered. The surface profile is shown in figure 10 for the case with $\kappa = 0$ (allowing for jumps in the slip) and $\kappa \to \infty$ using two different values of l/w_0. For $\kappa = 0$ there is only a slight difference in the profile for the two considered length scales, whereas the value of l/w_0 has a more major influence on the profiles at $\kappa \to \infty$. The profiles are qualitatively similar to results already displayed in figures 5 and 6 where the grains had the same orientation but different initial slip resistances.

Finally, a bicrystal with the grain orientations $\theta_{\mathrm{I}} = -15^\circ$ and $\theta_{\mathrm{II}} = 15^\circ$ and the same material parameters in each grain is studied. Figure 11 shows the surface profile for the two extreme cases $\kappa = 0$ and $\kappa \to \infty$ using two values of l/w_0. As discussed already for the

profile with $\theta_{\mathrm{I}} = 0^{\circ}$ and $\theta_{\mathrm{II}} = 15^{\circ}$, the value of l/w_0 has only a minor effect upon the surface shape for the choice $\kappa = 0$. An enhanced slip activity is evident near the interface for $\kappa = 0$ in figure 11, where the profile drops at the grain boundary creating a valley. It appears that the interface behaves as a free surface and dislocation activity is enhanced adjacent to it. The profile using $\kappa \to \infty$ creates a tip at the grain boundary. This tip becomes thinner and sharper with decreasing l/w_0.

6. Concluding remarks

The surface profile near a grain boundary of an aluminium sheet deformed in tension has been examined qualitatively in a scanning electron microscope. A local gradient in surface profile is observed within a few micrometres of the grain boundary.

Finite element calculations are reported here on the surface profile adjacent to a grain boundary in a bicrystal. The simulations are reported both for a strain gradient crystal plasticity formulation and for an isotropic, phenomenological strain gradient plasticity solid. A penalty to dislocations on each side of the grain boundaries has been introduced within the crystal plasticity formulation. The predicted profiles are very sensitive to the choice of grain boundary barrier to slip. In order to obtain physically realistic results for the surface profile, slip motion to the grain boundary must occur.

Acknowledgments

The work of UB is financially supported by the Danish Technical Research Council in a project entitled Modeling Plasticity at the Micron Scale.

References

Aifantis K E and Willis J R 2005 *J. Mech. Phys. Solids* **53**, 1047–70
Borg U, Niordson C F, Fleck N A and Tvergaard V 2006 *Int. J. Solids Struct.* **43** 4906–16
Borg U 2006 *Int. J. Plasticity* submitted
Evers L P, Brekelmans W A M and Geers M G D 2004 *Int. J. Solids Struct.* **41** 5209–30
Fleck N A and Hutchinson J W 2001 *J. Mech. Phys. Solids* **49** 2245–71
Fleck N A and Willis J R 2004 *J. Mech. Phys. Solids* **52** 1855–88
Gudmundson P 2004 *J. Mech. Phys. Solids* **52** 1379–406
Gurtin M E 2002 *J. Mech. Phys. Solids* **50** 5–32
Gurtin M E and Needleman A 2005 *J. Mech. Phys. Solids* **53** 1–31
Peirce D, Asaro R J and Needleman A 1983 *Acta Metall.* **31** 1951–76
Rice J R 1987 *Mech. Mater.* **6** 317–35
Stoudt M R and Ricker R E 2002 *Metall. Mater. Trans.* A **33** 2883–9
Wilson W R D and Lee W 2001 *J. Manuf. Sci. Eng.* **123** 279–83
Zhao Z, Radovitzky R and Cuitiño A 2004 *Acta Mater.* **52** 5791–804